

promoting access to White Rose research papers



Universities of Leeds, Sheffield and York
<http://eprints.whiterose.ac.uk/>

This is the author's post-print version of an article published in the **Journal of Non-Newtonian Fluid Mechanics**

White Rose Research Online URL for this paper:

<http://eprints.whiterose.ac.uk/id/eprint/76407>

Published article:

McIlroy, C, Harlen, OG and Morrison, NF (2013) *Modelling the jetting of dilute polymer solutions in drop-on-demand inkjet printing*. Journal of Non-Newtonian Fluid Mechanics, 201. 17 - 28. ISSN 0377-0257

<http://dx.doi.org/10.1016/j.jnnfm.2013.05.007>

Modelling the jetting of dilute polymer solutions in drop-on-demand inkjet printing

C. McIlroy, O.G. Harlen, N.F. Morrison.

Department of Applied Mathematics, University of Leeds, Woodhouse Lane, Leeds, LS2 9JT

Abstract

We have developed a simplified jetting model that predicts the printability of dilute, monodisperse polymer solutions in drop-on-demand (DoD) inkjet printing. Polymer molecules are modelled as finitely extensible non-linear elastic (FENE) dumbbells with fluid parameters chosen to fit the Zimm model. Three distinct jetting regimes are predicted, defined by the Weissenberg number Wi and the extensibility L of the molecules. The behaviour of the jet depends upon a critical factor that limits jet speed; regime 1 is restricted by fluid viscosity, regime 2 by elasticity and regime 3 by high strain extensional viscosity. We study two polymer solutions of disparate viscosity under different jetting conditions (i.e. print speed and nozzle geometry) and compare our results with experimental data and axisymmetric simulations. The maximum polymer concentration that can be jetted at a desired speed is found to scale with molecular weight M_w and is dependent on the solvent quality factor ν . We find that polymers can be stretched out in the print head for particular nozzle geometries, which has a considerable effect on the maximum polymer concentration that can be ejected. Furthermore, this ‘pre-stretch’ mechanism can fully extend molecules in the nozzle and consequently, molecules can undergo central scission due to high strain rates at the nozzle exit.

Key words: Polymer Solutions; inkjet printing, FENE model.

1 Introduction

The break-up of liquid jets is a classical problem in fluid mechanics (Eggers & Villermaux [16]) with a wide range of applications including spray painting, agricultural irrigation, pharmaceuticals and DNA sampling. In particular, inkjet printing has developed as a crucial technology for both graphical printing and digital fabrication through well-defined spatial deposition of solutions (Basaran *et al* [3], Derby [13], Hutchings and Graham [25]). The dynamics

of drop formation has been widely studied numerically using both one and two-dimensional approaches (Eggers & Dupont [15], Ambravaneswaran *et al.* [2], Wilkes *et al.* [35]). More recently, computational analysis of the drop-on-demand inkjet process has been developed e.g. Xu & Basaran [37], Morrison & Harlen [21].

In drop-on-demand (DoD) printing individual ink drops are ejected through a nozzle in response to an impulse. Understanding drop ejection behaviour via this technique is vital to the further development of inkjet technology (Feng [17]). The shape of a single drop upon exit is that of a nearly spherical bead with a trailing ligament (Martin *et al.* [26], Dong *et al.* [14]). Usually the size of the droplet ejected is equivalent to the nozzle diameter, however new experimental techniques have been developed to alter droplet radius (Chen & Basaran [8]). The trailing ligament may either retract into the main drop or breakup into small satellite drops. For Newtonian fluids, stable drop generation without satellites is limited to a narrow range of viscosities corresponding roughly to the Ohnesorge numbers in the range 0.1 to 1 (Derby [13], McKinley and Renardy [27]).

The addition of polymer molecules can significantly affect the breakup of liquid filaments generated by flow through a nozzle (Bazilevskii *et al.* [4], de Gans *et al.* [19], [20], Morrison & Harlen [21], Shore & Harrison [31]). In particular, the addition of small amounts of high-molecular-weight polymer can inhibit the formation of unwanted satellite drops so that the ligament retracts into the main drop. On the other hand polymer content affects the reliability of jetting; print speed may be compromised and, at high concentrations, the main drop may even fail to detach from the nozzle. There exists a critical polymer concentration threshold at which printing at the desired speed is possible, within the limit of the print head drive.

Hoath *et al.* [24] have recently analysed experimental results on the jetting behaviour for mono-disperse, linear polystyrene dissolved in two solvents of disparate viscosity, jetted through different nozzle diameters at different print speeds. They introduce a simple model (based on one originally proposed by Bazilevskii *et al.* [4]), in which the fluid is modelled as a solution of finitely extensible dumbbells (FENE model) and the parameters are chosen to fit the Zimm model (Clasen *et al.* [11]). Although the polymers present in ink formulations are rarely linear (Xu *et al.* [36]), the model system was chosen to determine how the polymer concentration threshold, at which jetting at the desired speed is possible, varies with molecular weight. Three regimes of jetting behaviour are defined by the dominant mechanism that limits jet speed; regime 1 is restricted by zero-shear viscosity, regime 2 by viscoelasticity and regime 3 by high strain rate extensional viscosity. The transitions between these regimes are determined by the initial Weissenberg number $Wi_0 = U_0\tau/D$, where U_0 is the jet velocity at the nozzle exit, τ is the fluid relaxation time and D is

the nozzle diameter. The first transition from regime 1 to 2 occurs at $Wi_0 = 1/2$, at which point polymers can become significantly extended from their equilibrium configuration. The second transition from regime 2 to 3 occurs at $Wi_0 = L$, when polymers reach their finite extensibility limit L .

In their paper, Hoath *et al.* demonstrated agreement of the scaling of the maximum jettable concentration with molecular weight predicted in these jetting regimes with experimental data. However, they did not perform a quantitative comparison. The aim of this paper is to explore these jetting regimes and the transitions between them numerically for two different polymer systems, and to make a quantitative comparison with experimental measurements.

Flow-induced deformations can lead to irreversible changes in the structure of a polymeric fluid; if the rate of extension far exceeds the rate of relaxation, then the polymer chain can be broken. Mechanical degradation of polymers in extensional flow has long been recognised (Odell & Keller [30]) and leads to a reduction in the average molecular weight. A-Alamry *et al.* [1] have recently reported evidence of flow-induced polymer degradation in DoD jetting. Central scission is observed for polystyrene in a number of good solvents under certain jetting conditions for a bounded range of molecular weights. Since only those molecules that are fully extended can be fractured at the centre of the polymer chain (Muller *et al.* [29]), in this paper we investigate whether flow-induced central scission is possible under the conditions of DoD jetting.

2 Modelling Drop on Demand Jetting

The velocity \mathbf{u} of a general fluid with density ρ and pressure p is described by the usual conservation of momentum equation

$$\rho \frac{D\mathbf{u}}{Dt} = -\nabla p + \nabla \cdot \boldsymbol{\sigma}, \quad (1)$$

along with the incompressible condition.

$$\nabla \cdot \mathbf{u} = 0. \quad (2)$$

Here $\frac{D}{Dt}$ denotes the Lagrangian material derivative. The stress tensor $\boldsymbol{\sigma}$ is determined by the choice of constitutive model.

2.1 Constitutive Model

A simple constitutive model for describing dilute polymer solutions in extensional flow is the finitely extensible non-linear elastic dumbbell model with the Chilcott-Rallison closure approximation [9], also known as the FENE-CR model. In the FENE-CR model, the total stress is given by

$$\boldsymbol{\sigma} = 2\mu_s\mathbf{E} + Gf(\mathbf{A} - \mathbf{I}),$$

where μ_s is the solvent viscosity, \mathbf{E} is the strain rate tensor and the polymer stress consists of the elastic modulus G , the conformation tensor \mathbf{A} and the FENE factor

$$f = \frac{L^2}{L^2 + 3 - \text{tr}(\mathbf{A})}, \quad (3)$$

that accounts for the finite extensibility L of the polymer chain. The conformation tensor \mathbf{A} satisfies the evolution equation

$$\frac{D\mathbf{A}}{Dt} = \mathbf{K} \cdot \mathbf{A} + \mathbf{A} \cdot \mathbf{K}^T - \frac{f}{\tau}(\mathbf{A} - \mathbf{I}), \quad (4)$$

where τ is the relaxation time of the polymer and $K_{ij} = \frac{\partial u_i}{\partial x_j}$ is the velocity gradient tensor.

For a dilute, monodisperse polymer solution the parameters in the FENE-CR model, namely elastic modulus G , relaxation time τ and finite extensibility L , can be determined as functions of the molecular weight M_w , weight fraction concentration ϕ and solvent quality factor ν using Zimm theory (Clasen *et al.* [11]). The elastic modulus is proportional to concentration and inversely proportional to molecular weight

$$G = \frac{\phi RT}{M_w}, \quad (5)$$

where R is the universal gas constant and T is the absolute temperature. The relaxation time τ of the dumbbell is chosen to be the longest Zimm time and is defined as

$$\tau = \frac{1}{\Lambda} \frac{[\mu]\mu_s M_w}{RT}, \quad (6)$$

where $\Lambda = \hat{\tau}/\tau = \sum_i i^{-3\nu}$ is the universal ratio of the characteristic relaxation time $\hat{\tau}$ to the longest relaxation time τ . The intrinsic viscosity $[\mu]$ is described by the Mark-Houwink relation

$$[\mu] = KM_w^{3\nu-1}, \quad (7)$$

where K is a constant dependent upon the polymer system. The finite extensibility L can be determined from the ratio of the equilibrium coil to the fully

extended length of the polymer so that

$$L^2 = 3 \left(\frac{j \sin^2(\theta/2) M_w}{C_\infty M_u} \right)^{2(1-\nu)}, \quad (8)$$

where θ is the carbon-carbon bond angle, j is the number of bonds of a monomer unit with molar mass M_u and C_∞ is the characteristic ratio. It should be noted that there is experimental evidence [32] suggesting that this equation over predicts the finite extensibility of a molecule. For Zimm theory to be valid we require that

$$\phi/\phi^* \ll 1, \quad (9)$$

where ϕ^* is the critical overlap concentration.

Hence, for a dilute mono-disperse polymer solution, the FENE-CR model parameters scale with molecular weight as

$$G \sim M_w^{-1} \quad ; \quad \tau \sim M_w^{3\nu} \quad ; \quad L \sim M_w^{(1-\nu)}, \quad (10)$$

derived from equations (5), (6), (7) and (8). As an example, polystyrene dissolved in acetophenone (ATP), a good solvent with a quality factor of $\nu = 0.59$, has relaxation time

$$\tau = \frac{M_w^{1.77}}{3.24 \times 10^8} \mu\text{s}, \quad (11)$$

and finite extensibility

$$L^2 = \frac{M_w^{0.82}}{9.2 \times 10^3}, \quad (12)$$

for a molecular weight M_w measured in Daltons (Da).

2.2 A Simple Jetting Model

In their recent paper, Hoath *et al.* [24] describe a simple model for predicting the printability of polymeric fluids as illustrated in Figure 1. After ejection from the nozzle, the main drop is slowed down by the extensional flow in the connecting fluid ligament. We assume that a drop of density ρ and volume V_{drop} is ejected from a nozzle of diameter D , at speed U_0 , which we define as the speed of the main drop when it is a distance D from the nozzle exit. The main drop is connected to the nozzle by a ligament of volume V_{lig} and initial length D . The volume of fluid in the drop and the ligament is assumed to remain constant and the ligament is assumed to deform uniformly as its length Z increases. The main drop slows down to final velocity U_f .

For this simplified jetting model, we have the following governing equations

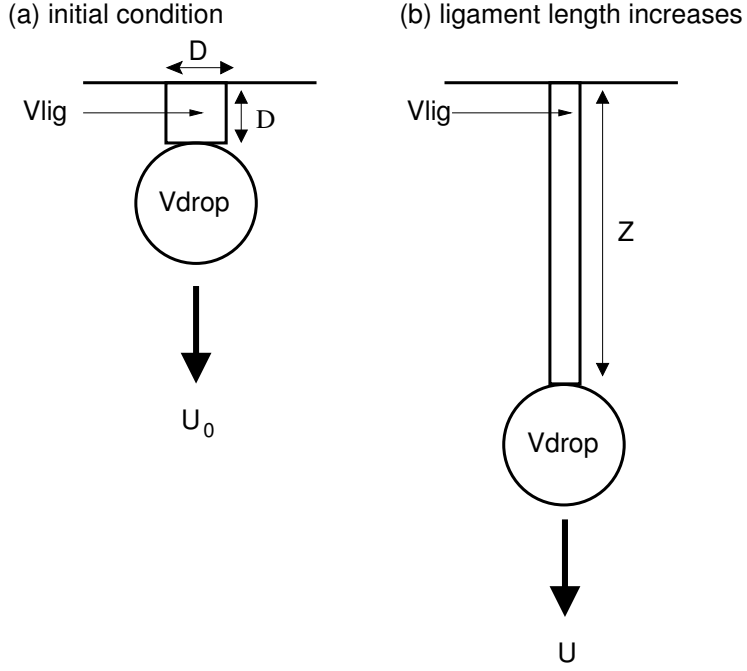


Fig. 1. Simplified model of drop-on-demand printing. The main drop slows down from velocity U_0 in (a) to velocity U in (b). The ligament increases from initial length D in (a) to length Z in (b).

[24]. The speed of the drop is given by

$$U = \frac{dZ}{dt}.$$

and the strain-rate $\dot{\epsilon} = U/Z$. Assuming that the only forces acting on the drop are from the stress difference in the ligament, the drop velocity satisfies the force balance

$$\rho V_{drop} \frac{dU}{dt} = -\frac{V_{lig}}{Z} \left(\frac{3\mu_s U}{Z} + Gf(A_{zz} - A_{rr}) \right).$$

The force consists of a viscous and polymer contribution multiplied by the cross-sectional area of the jet. From equation (4), the configuration tensor components A_{zz} and A_{rr} satisfy the evolution equations

$$\begin{aligned} \frac{dA_{zz}}{dt} &= \left(\frac{2U}{Z} - \frac{f}{\tau} \right) A_{zz} + \frac{f}{\tau}, \\ \frac{dA_{rr}}{dt} &= - \left(\frac{U}{Z} + \frac{f}{\tau} \right) A_{rr} + \frac{f}{\tau}. \end{aligned} \tag{13}$$

These equations are non-dimensionalised using relaxation time τ as the unit of time and nozzle diameter D as the length scale. Hence, for dimensionless veloc-

ity u and dimensionless length z we have the following set of non-dimensional governing equations:

$$\begin{aligned}
u &= \frac{dz}{dt}, \\
\frac{du}{dt} &= -\frac{El^*}{z} \left(\frac{3u}{z} + cf(A_{zz} - A_{rr}) \right), \\
\frac{dA_{zz}}{dt} &= \left(\frac{2u}{z} - f \right) A_{zz} + f, \\
\frac{dA_{rr}}{dt} &= -\left(\frac{u}{z} + f \right) A_{rr} + f.
\end{aligned} \tag{14}$$

together with the initial conditions,

$$u = Wi_0 = \frac{U_0\tau}{D} \quad \text{and} \quad z = A_{zz} = A_{rr} = 1, \quad \text{at} \quad t = 0.$$

In our dimensionless units, the velocity at time zero is equal to the initial Weissenberg number, Wi_0 . The Weissenberg number at time t is given by $Wi = U\tau/Z = u/z$ and is a decreasing function of time as the length of the ligament z increases. Thus, even if the initial Weissenberg number is large, the extension rate in the ligament will drop below the coil-stretch transition by the time that the ligament has grown to dimensionless length of $2Wi_0$.

The dimensionless number that determines the deceleration of the drop is the modified elasticity number El^* , defined as

$$El^* = \frac{V_{lig}}{V_{drop}} \frac{Wi_0}{Re} = \frac{V_{lig}}{V_{drop}} \frac{\mu_s\tau}{\rho D^2}.$$

This is a combination of the Reynolds' number

$$Re = \frac{\rho U_0 D}{\mu_s},$$

giving a measure of the viscous forces compared to the inertial forces and the initial Weissenberg number, Wi_0 defined as above. The pre-factor V_{lig}/V_{drop} appearing in the modified elasticity number is assumed to be 1/4 based on observations in both simulations and experiments that approximately 80% of the fluid ejected from the nozzle ends up in the main drop.

The dimensionless polymer concentration c is given by

$$c = \frac{G\tau}{\mu_s}.$$

This is equivalent to the dimensionless grouping ϕ/ϕ^* . The molecular weight scalings of the initial Weissenberg number and the dimensionless concentration

c can be derived from the Zimm scalings (10) to be

$$Wi_0 \sim M_w^{3\nu} \quad ; \quad c \sim M_w^{3\nu-1}. \quad (15)$$

For comparison with both experiments and axisymmetric simulations, the initial conditions of the simplified jetting model correspond to the time at which the fluid exits the nozzle, i.e. the model velocity U_0 corresponds to the velocity at which the drop exits the nozzle. This velocity is higher generally by a factor of 1.5 to 3 times the final velocity U_f (see Hoath *et al.* [23]), which is the drop speed measured at an order of 1 mm from the nozzle exit.

The governing equations (14) are solved numerically to calculate the ‘maximum jettable concentration’ as a function of molecular weight. This concentration is defined to be the maximum polymer content that can be ejected from the print head with a particular desired value of U_f . In terms of the jetting model, the maximum jettable concentration is taken to be the concentration at which the specified ratio U_0/U_f is achieved.

This simple model has a number of limitations. First, the model neglects the nozzle geometry and any subsequent effects due to the flow through the nozzle. Consequently, the model assumes that the polymers are initially at equilibrium i.e. $\mathbf{A}^0 = \mathbf{I}$. Second, the model does not take into account the break-off of the ligament from the nozzle.

2.3 Asymptotic Predictions of the Simple Jetting Model

To determine the three jetting regimes, as derived by Hoath *et al.* [24], we consider the asymptotic limits of the force balance equation

$$\frac{1}{Wi_0} \frac{du}{dt} = -\frac{1}{4Re} \left(\frac{3u}{z^2} + \frac{cf}{z} (A_{zz} - A_{rr}) \right), \quad (16)$$

as given in the governing equations (14).

In jetting regime 1 the initial Weissenberg number Wi_0 is small such that the extension rate in the ligament $u/z \ll 1$. So in this limit,

$$A_{zz} \sim 1 + 2u/z, \quad A_{rr} \sim 1 - u/z, \quad f = 1,$$

and the force balance equation (16) reduces to

$$\frac{1}{Wi_0} \frac{du}{dt} = -\frac{1}{4Re} \left(\frac{3u}{z^2} (1 + c) \right).$$

The fluid behaviour is Newtonian with a viscosity given by

$$\mu_0 = \mu_s(1 + c).$$

Thus, the maximum polymer concentration that can be jetted at a particular molecular weight is limited by the increase in the zero-shear rate viscosity and the reduction in drop velocity scales with molecular weight via (15)

$$-\Delta u \sim \frac{c}{Re} \sim M_w^{3\nu-1}.$$

Jetting regime 2 is defined to be the regime in which the initial Weissenberg number satisfies $1/2 < Wi_0 < L$. In this case, the initial extension rate is strong enough to stretch the polymer molecules and fluid behaviour is viscoelastic. However, as the strain increases, the maximum value of A_{zz} remains. We assume that the polymers will relax before becoming fully extended and so the FENE factor can again be approximated by $f \approx 1$. Assuming that $1 \ll A_{zz} \ll L^2$, the dumbbell evolution equation (14) can be integrated to give

$$A_{zz} \approx z^2 e^{-t},$$

and so the force balance equation (16) reduces to

$$\frac{1}{Wi_0} \frac{du}{dt} = -\frac{1}{4Re} \left(\frac{3u}{z^2} + c(z e^{-t}) \right).$$

Integrating along the ligament length from 1 to z , the reduction in drop velocity is given by

$$\frac{\Delta u}{Wi_0} = -\frac{1}{4Re} \left(3 \left(1 - \frac{1}{z} \right) + c \int_0^t z(t) e^{-t} dt \right).$$

Recalling that the Weissenberg number is equivalent to the dimensionless velocity, the integral can be approximated by taking $z = 1 + Wi_0 t$ and the limit $z \rightarrow \infty$

$$\int_0^\infty z e^{-t} dt = 1 + Wi_0.$$

The reduction in drop velocity is thus given by

$$\frac{\Delta u}{Wi_0} = -\frac{1}{4Re} (3 + c(1 + Wi_0)),$$

which has the molecular weight scaling (15),

$$-\Delta u \sim \frac{c Wi_0}{Re} \sim M_w^{6\nu-1}.$$

In jetting regime 3, defined by $Wi_0 > L$, the polymer chains reach their finite

extension limit and the fluid then behaves like a suspension of rigid rods. Assuming that $A_{zz} \rightarrow L^2$, the dumbbell evolution equation (14) is approximated as

$$fA_{zz} \approx \frac{u}{z}L^2,$$

and so the force balance equation (16) reduces to

$$\frac{1}{Wi_0} \frac{du}{dt} = \frac{1}{4Re} (3 + 2cL^2) \frac{u}{z^2} \sim \left(\frac{u}{z^2}\right) cL^2.$$

Integrating along the fully extended ligament length from L to $z \rightarrow \infty$ gives the reduction in drop velocity

$$-\Delta u \sim \frac{cL}{Re} \sim M_w^{2\nu},$$

using the molecular weight scalings given in equations (10) and (15).

Thus, by using the Zimm model to determine the molecular weight dependence of the relaxation time we can determine how the maximum jettable polymer concentration scales with molecular weight during each of the three jetting regimes. These scalings laws are summarised in Table 1.

Concentration	Regime 1	Regime 2	Regime 3
wt%	$M_w^{1-3\nu}$	$M_w^{1-6\nu}$	$M_w^{-2\nu}$
c	1	$1/Wi_0$	$1/L$

Table 1
Regime scalings in terms of different concentrations.

The transition from regime 1 to regime 2 occurs at $Wi_0 = 1/2$ and corresponds to the molecular weight at which coil-stretch transition will occur during the jetting process. The transition from regime 2 to regime 3 occurs at $Wi_0 = L$, at which polymers of this molecular weight reach their finite extension limit during jetting. The transitions depend upon jetting conditions such as drop speed and nozzle diameter, as well as polymer characteristics and the solvent viscosity.

3 Jettable Concentration Thresholds

In order to test whether these asymptotic regimes exist in practice, we have calculated numerical solutions to the governing equations (14) for parameter values chosen to match the experimental systems studied by de Gans *et al.*

[18] and Hoath *et al.* [22]. These calculations were performed using MATLAB.

3.1 Polystyrene/ATP Solution jetted using the AutoDrop System

The fluids studied by de Gans *et al.* [18] were solutions of polystyrene dissolved in acetophenone (ATP) jetted at $U_f = 2$ m/s from a $70 \mu\text{m}$ diameter nozzle using an AutoDrop system. The AutoDrop system, manufactured by micro-drop technologies, uses a standard micropipette for the nozzle. The speed of the jet on exiting the nozzle is unknown for this case. We estimate that the ratio between final jet speed and the speed at which the ink exits the nozzle for a micropipette to be 1.5 by fitting the jetting model to the experimental data at low molecular weight where the fluid is Newtonian. Thus, in the jetting model we assume $U_0 = 3$ m/s. The solvent ATP is of low-viscosity ($\mu_s = 0.0017$ Pa.s) and is classed as ‘good’, with solvent quality factor $\nu = 0.59$. The jetting conditions and fluid parameters are listed in Table 2.

Nozzle	Micropipette	Solvent	ATP
nozzle diameter, D	$70 \mu\text{m}$	solvent viscosity, μ_s	0.0017 Pa.s
initial speed, U_0	3 m/s	quality factor, ν	0.59
print speed, U_f	2 m/s	fluid density, ρ	1028 kg/m ³

Table 2

Jetting conditions and fluid parameters for polystyrene dissolved in ATP jetted from an AutoDrop system chosen to correspond with experimental data [18].

Figure 2 demonstrates the change in zz -component of the configuration tensor as molecular weight is increased. For low molecular weights ($M_w = 100$ kDa), the A_{zz} remains small, indicating that the flow is not strong enough to deform the polymer molecules. Thus, the axial stress is proportional to the strain rate and jettability depends on the fluid viscosity. For intermediate molecular weights ($M_w = 1000$ kDa), A_{zz} initially grows but then relaxes before reaching its finite extensibility limit $L^2 = 762$. Thus, the deformation remains within the Oldroyd limit where $A_{zz} \ll L^2$ and jettability is limited by viscoelasticity. For large molecular weights ($M_w = 7000$ kDa), A_{zz} approaches the finite extensibility limit $L^2 = 3783$, indicating that polymer molecules do reach their finite extension.

In the steady state equilibrium $dA_{zz}/dt = 0$, the FENE factor given by equation (3) balances the stretching by the velocity gradient. So, in the limit $A_{zz} \gg 1$, the dumbbell evolution equation given by equation (13) reduces

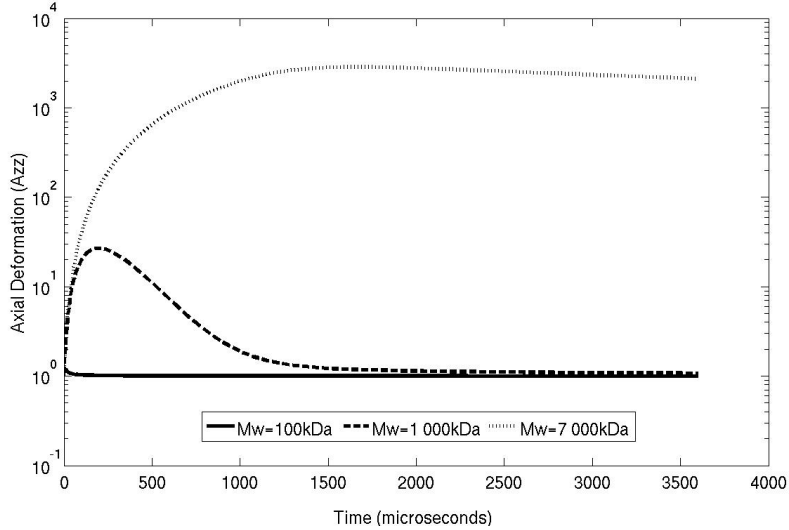


Fig. 2. A_{zz} profiles for molecular weights $M_w = 100$ kDa (solid), $M_w = 1000$ kDa (dash) and $M_w = 7000$ kDa (dot) for polystyrene in ATP jetted from an AutoDrop system.

to

$$0 = \left(2\dot{\epsilon} - \frac{f}{\tau} \right) A_{zz},$$

and the FENE factor can be approximated as $f = 2\dot{\epsilon}\tau$. Thus, in this steady state, the axial stress component can be written as

$$\frac{A_{zz}}{L^2} = 1 - \frac{1}{2Wi}.$$

Provided that $Wi > 1/2$, it is the non-linear spring that is responsible for the relaxation of the axial stress. The molecules do not recoil, but remain in a fully extended equilibrium. Consequently, jettability is limited by high strain rate extensional viscosity rather than molecule elasticity.

Figure 3 shows the maximum jettable concentration predicted by the jetting model in terms of the dimensionless concentration (c) compared to the initial Weissenberg number Wi_0 . In this case, the maximum jettable concentration is considered to be the ejected concentration at which the ratio $U_0/U_f = 1.5$ is achieved. The numerical calculations demonstrate the three jetting regimes with asymptotic scaling laws Wi_0^0 , Wi_0^{-1} and L^{-1} , respectively.

Hoath *et al.* [24] define the transition from the Newtonian regime to the viscoelastic regime by $Wi_0 = 1/2$. The corresponding molecular weight at which

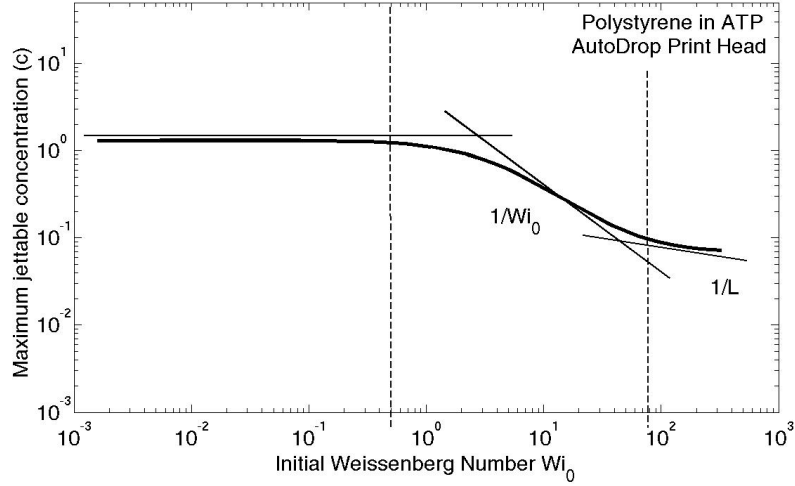


Fig. 3. Maximum jettable concentration (c) of polystyrene in ATP jetted using an AutoDrop system predicted by the jetting model (curve). Predicted asymptotic scaling laws for each regime (lines). Transitions between regimes (dashed) calculated from Zimm theory.

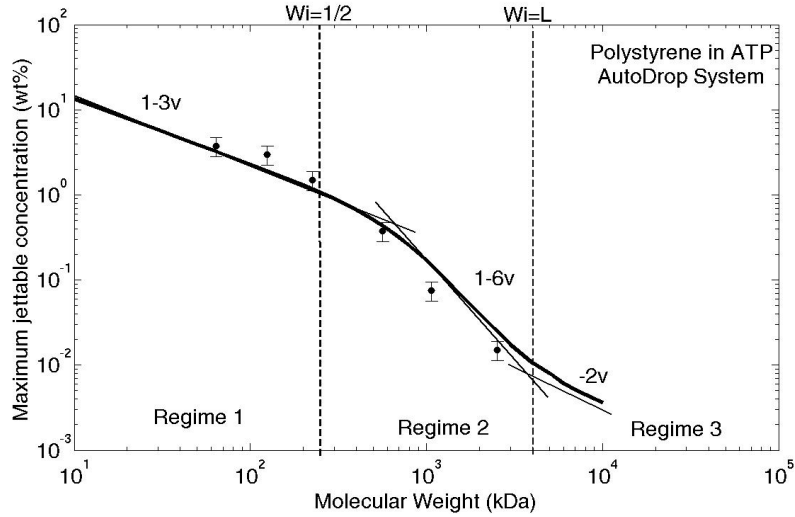


Fig. 4. Maximum jettable concentration (wt%) of polystyrene in ATP jetted using an AutoDrop system predicted by the jetting model (curve). Experimental results [24] (circles) assuming a 25% error bar. Transitions between regimes (dashed) calculated from Zimm theory.

this transition occurs is calculated using the Zimm relaxation time (11) to be

$$M_w = \left(\frac{1}{2} \frac{D}{U_0} 3.24 \times 10^8 \right)^{1/3\nu} \approx 258 \text{ kDa.}$$

At this molecular weight, although the initial strain rate exceeds the coil-

stretch transition ($\dot{\epsilon}_0\tau = 1/2$), the strain rate then drops below critical so that the polymers have not uncoiled for a sufficient amount of time to allow viscoelasticity to fully dominate. Thus, the transition from regime 1 to regime 2 occurs at a higher molecular weight than predicted by $Wi_0 = 1/2$. The second transition from regime 2 to 3 at $Wi_0 = L$ is calculated using the Zimm relaxation time (11) and finite extensibility (12) to be

$$M_w = \left(\sqrt{9.2 \times 10^{-3}} \frac{D}{U_0} 3.24 \times 10^8 \right)^{1/(4\nu-1)} \approx 3273 \text{ kDa.}$$

Figure 4 compares the maximum jettable concentration (wt%) that can be jetted experimentally [24] with that predicted by the jetting model. The experimental results agree well with the model predictions and follow the asymptotic scaling laws $M_w^{1-3\nu}$ and $M_w^{1-6\nu}$, respectively. However, the data does not extend into regime 3.

3.2 Polystyrene/DEP Solution jetted using the Xaar Print head

We now consider the system studied by Hoath *et al.* [22] in which polystyrene dissolved in diethylphthalate (DEP) is jetted at $U_f = 6$ m/s from a 50 μm diameter nozzle using a Xaar XJ126-200 print head. Hoath *et al.* [23] show that the actuation pulse used in the Xaar print head typically produces a ratio of 2-3 between the drop speed upon exiting the nozzle and the final drop speed measured at a distance of 1 mm from the nozzle exit. Here we will take the ratio as 3, thus we have $U_0 = 18$ m/s in the jetting model. The solvent DEP has a higher viscosity than ATP ($\mu_s = 0.01$ Pa.s) and is also classed as ‘good’, with a similar solvent quality factor $\nu = 0.567$. The jetting conditions and fluid parameters are listed in Table 3.

Nozzle	Xaar	Solvent	DEP
nozzle diameter, D	50 μm	solvent viscosity, μ_s	0.01 Pa.s
initial speed, U_0	18 m/s	quality factor, ν	0.567
print speed, U_f	6 m/s	fluid density, ρ	1117 kg/m ³

Table 3

Jetting conditions and fluid parameters for polystyrene dissolved in DEP jetted from a Xaar XJ126-200 print head chosen to correspond with experimental data [22].

Figure 5 shows the maximum jettable concentration (c), on the assumption that the ratio $U_0/U_f = 3$ is achieved [23]. The results follow the predicted asymptotic scaling laws Wi_0^0 and L^{-1} for jetting regimes 1 and 3, respectively.

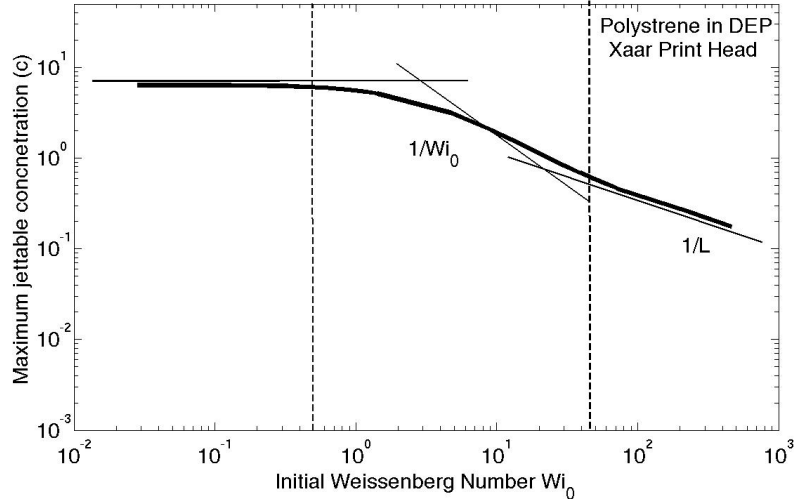


Fig. 5. Maximum jettable concentration of polystyrene (c) in DEP from the Xaar print head predicted by the jetting model (solid curve). Predicted scaling laws for each regime (lines). Transitions between regimes (dashed) calculated from Zimm theory.

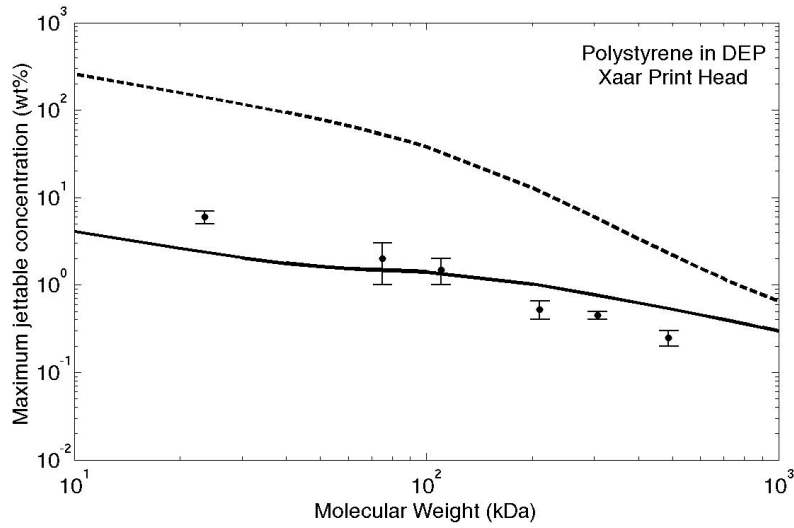


Fig. 6. Maximum jettable concentration of polystyrene (wt%) in DEP from the Xaar print head predicted by the jetting model (dashed curve) compared to the corrected jetting model (solid curve). Experimental results [24] with error bars (circles).

However, the middle regime asymptote of Wi_0^{-1} is not achieved. Again using Zimm values for relaxation time and finite extensibility, the first transition from regime 1 to 2 is predicted to occur at approximately $M_w = 54$ kDa and the second transition from regime 2 to 3 is predicted to occur at $M_w = 608$ kDa. In this case, the Weissenberg numbers for a particular molecular weight

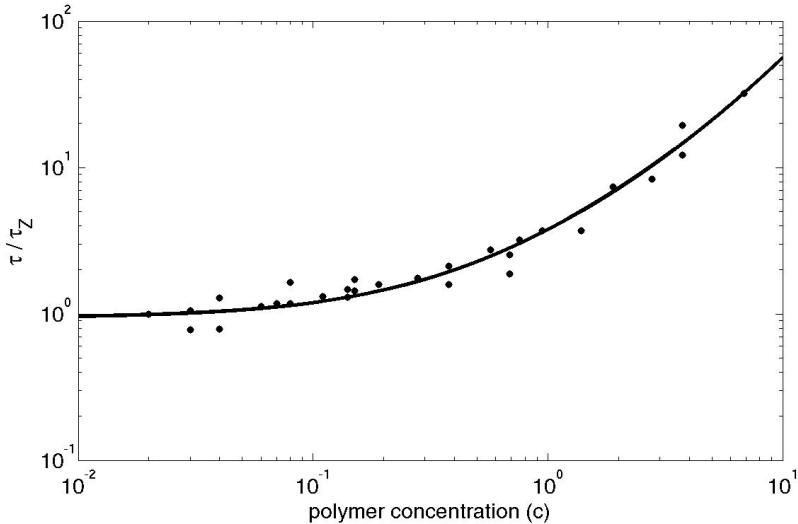


Fig. 7. The measured relaxation time τ compared to the Zimm relaxation time τ_Z (6) is shown as a function of concentration c , as given in [33], for a range of molecular weights $M_w = 70 - 488$ kDa (circles).

are larger due to the higher solvent viscosity of DEP and faster jetting speed of the Xaar print head. Consequently, the second transition occurs at a low molecular weight, so that L is not large enough to give a sufficient range of Weissenberg numbers for regime 2 to fully develop.

Figure 6 shows the maximum jettable concentration (wt%) predicted by the jetting model (dashed line) significantly overestimates the experimental data [24]. There are two partial explanations for this discrepancy.

First, we have assumed that the relaxation time is given by the Zimm model and is independent of concentration. However, Vadillo *et al.* [33] measure the relaxation time for polystyrene in DEP and find that it increases with concentration for ϕ close to ϕ^* . This data is shown in Figure 7 for molecular weight range $M_w = 70 - 488$ kDa, where the experimentally measured relaxation time τ is compared to the Zimm relaxation time τ_Z given by equation (6). The relaxation time at a dimensionless concentration $c = 1$ is about a factor of 3 larger than the Zimm time. The relaxation time (6) defined in the jetting model is adjusted according to the line of the best fit shown in Figure 7 (second order polynomial). In making this correction, the predicted concentration threshold is reduced and is much closer to the experimental data, as shown in Figure 6.

Even with this correction, at high molecular weights ($M_w > 100$ kDa) the jetting model continues to overestimate the experimental data. This is in contrast to the ATP/micropipette system where we find good quantitative agreement. A possible explanation for this discrepancy is pre-stretch of the polymers due

to the print head geometry. The AutoDrop system uses a micropipette nozzle, which tapers gently to the nozzle exit, whereas the Xaar print head has a sudden contraction. Consequently, the contraction flow into the nozzle may extend the polymers before they are subjected to the extensional flow during jetting. Similar issues were suspected for the Dimatix DMP print head used by A-Alamry *et al.* [1], which we will discuss in section 5.

Evidence of polymers subjected to pre-stretch in a nozzle has previously been observed experimentally by Clasen *et al.* [12] in the study of the dripping to jetting transition. This transition has also been studied numerically using a simplified jetting model (Clanet & Lasheras [10]). Pre-stretch was seen to prevent the occurrence of first stage inertio-capillary thinning of a liquid jet and, for very small nozzles, even prohibit the establishment of the viscoelastic thinning regime. To investigate the effect of pre-stretch requires full simulations of the flow within the nozzle.

4 Full Axisymmetric Simulations

4.1 Simulation Method

We compare our simple jetting model with full axisymmetric simulations of the jet breakup. The simulations employed here use the Eulerian-Lagrangian finite-element method (Harlen *et al.* [28]) and have previously been used to study jet breakup in drop-on-demand printing for both Newtonian (Casterjón-Pita *et al.* [7]) and viscoelastic (Morrison & Harlen [21]) fluids.

The software uses a moving-mesh, finite-element method to solve the momentum equation (1) and conservation of mass (2). By allowing the finite elements to deform with the fluid velocity, the FENE dumbbell evolution equation (4) is solved in the co-deforming frame in which the time derivative is the upper-convected derivative. At the ink-air interface the boundary condition is defined to be

$$[\sigma \cdot \hat{\mathbf{n}}]_{air}^{ink} = -\gamma \left(\frac{1}{R_1} + \frac{1}{R_2} \right) \hat{\mathbf{n}},$$

where $\hat{\mathbf{n}}$ is the unit vector normal to the interface, γ denotes surface tension and R_1, R_2 are the principle radii of curvature. Further details of the numerical scheme can be found in references [28] and [34].

The nozzle geometry used in the axisymmetric simulations is detailed in Figure 8. The jet is assumed to be axisymmetric such that a 2D coordinate system may be employed to fully describe the jet dynamics. The axis of symmetry lies at the centre of the outlet nozzle. The nozzle shape and dimensions considered

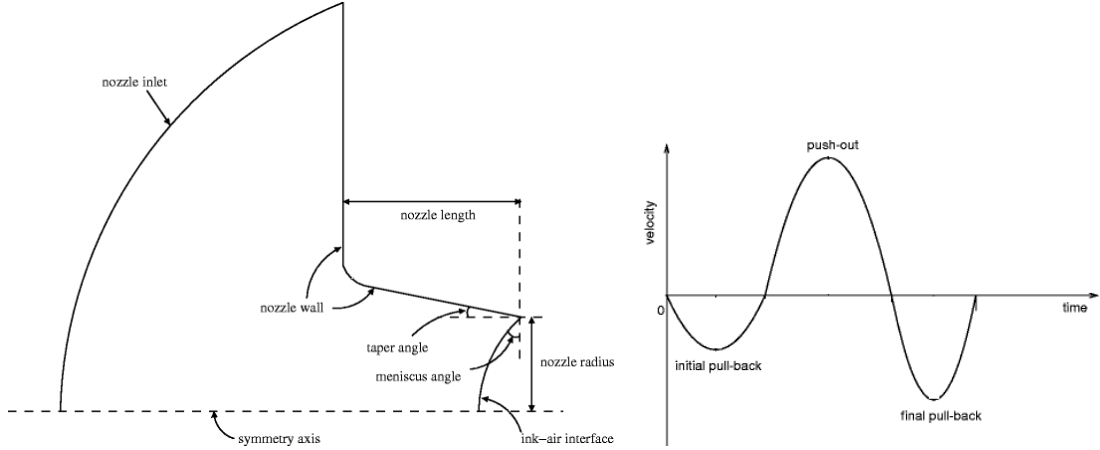


Fig. 8. Left: Nozzle geometry used in axisymmetric simulations. Right: Initial velocity profile/driving signal applied to the curved nozzle inlet.

here are based on the Xaar XJ126-200 print head used by Hoath *et al.* [24]. The simulations only consider the contraction flow into the nozzle and do not model the details of the print head itself, which is non-axisymmetric.

The fluid is driven by imposing a time dependent velocity profile on the curved inlet boundary upstream of the nozzle. The driving signal is based upon the profile used by Morrison & Harlen [21] and consists of three stages known as the ‘pull-push-pull’ curve, as shown in Figure 8. This profile is chosen to match the flow conditions of the Xaar print head near to the nozzle outlet, although some DoD printers use a push only profile. The initial ‘pull’ phase draws fluid into the print head from the nozzle outlet, the following ‘push’ phase ejects the fluid from the nozzle and the final ‘pull’ phase draws back the trailing ligament to ensure that it breaks primarily at the nozzle.

Figure 9 shows a time series from a simulation of Newtonian jet generation and breakup. The initial pull phase of the driving signal is shown in Figure 9(a). The velocity U_0 defined in the simplified jetting model corresponds to the tip velocity when the ligament length and diameter are equal (and equal to the nozzle diameter). This occurs at the beginning of the final ‘pull’ stage of the simulated driving signal and can be seen in Figure 9(b). The ligament is then seen to break off from the nozzle at the end of this ‘pull’ phase in Figure 9(c). The final velocity U_f defined in jetting model is the speed that the front of the main drop reduces to. This is usually measured at 1 mm from the nozzle exit and corresponds to Figure 9(d). However, the velocity after break off from the nozzle is approximately constant across Figures 9(c-e).

After break off from the nozzle, the trailing ligament may merge with the main drop or breakup due to the capillary instability. The front drop, which is the drop of greatest volume, is referred to as the main drop and any subse-

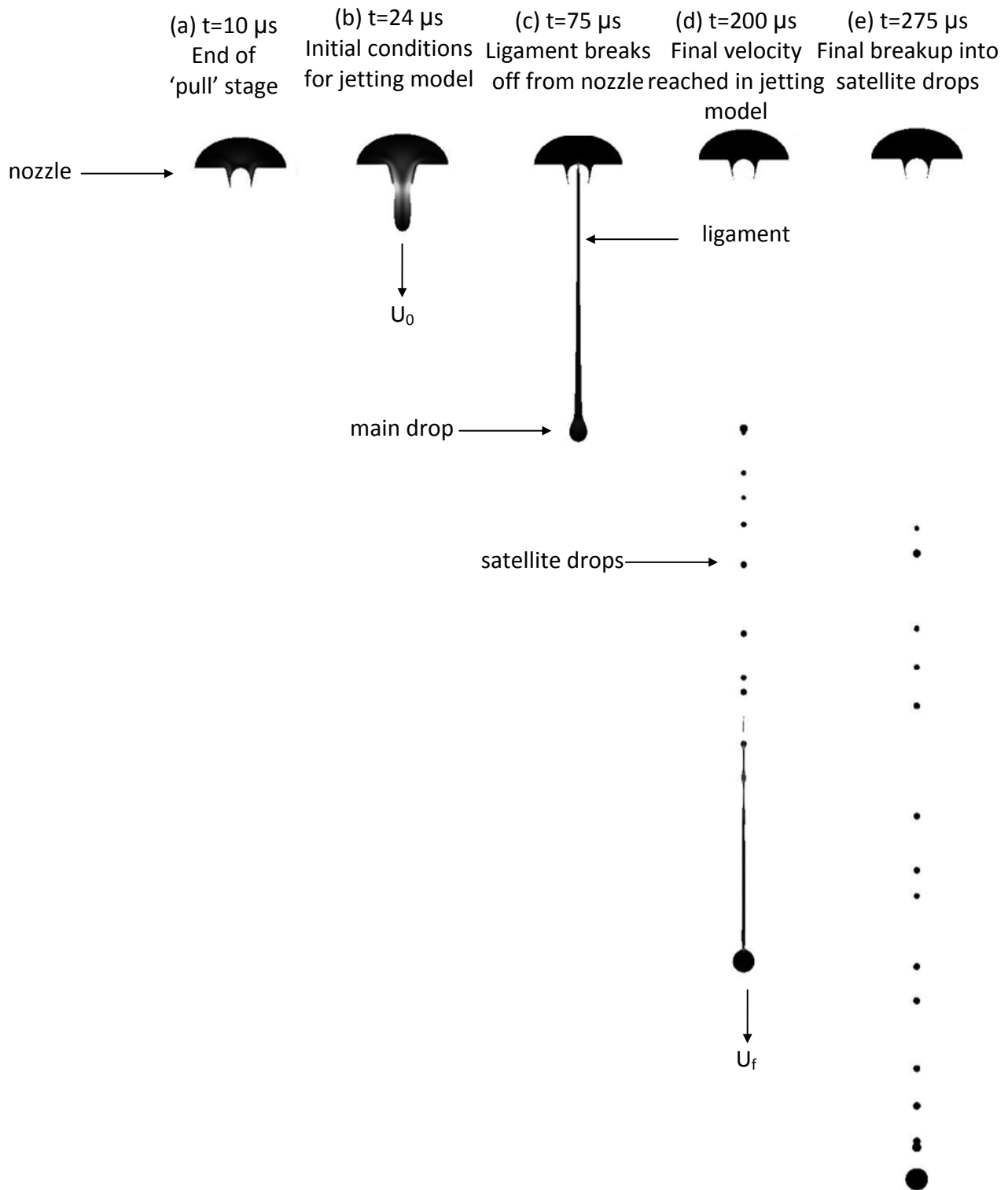


Fig. 9. Simulation of the different phases of jet generation for a low molecular weight polymer solution in a high-viscosity solvent.

quent droplets generated by ligament breakup are called satellite drops. The generation of satellite drops is dependent on a number of factors, notably the Ohnesorge number, and for polymeric fluids the concentration and the molecular weight have significant effects on both the number and the size of the satellite drops produced [21]. In counting the satellite drop volume in our simulations, no post-breakup coalescence is considered, whereas in reality drops may merge into one another. The ligament is seen to breakup into numerous satellite drops in Figure 9(e).

4.2 Comparison to Axisymmetric Simulations

In order to explain the discrepancies between the jetting model and the experimental data discussed in section 3.2, we have performed full axisymmetric simulations of a polystyrene/DEP system jetted from a Xaar print head. Simulations of each jetting regime are shown in Figure 10. The molecular weights chosen to represent each regime are listed in Table 4 along with the maximum jettable concentration predicted by the simulations. The solvent parameters and jetting conditions used for these simulations correspond to those detailed in Table 3.

	M_w (kDa)	Wi_0	Polymer conc. (wt%)	Polymer conc. (c)
Regime 1	50	0.4	3%	0.47
Regime 2	200	4.6	0.095%	0.04
Regime 3	2000	232	0.003%	0.005

Table 4

Molecular weights chosen to represent each jetting regime and maximum jettable concentrations predicted by the axisymmetric simulations.

Figure 10 demonstrates the distinct jetting behaviours of each regime. In regime 1, the breaking behaviour is similar to that of a Newtonian fluid. Break off from the nozzle occurs earlier than in the other regimes, as expected, and the ligament undergo capillary thinning, subsequently breaking into a number of satellite drops. In the second jetting regime the ligament becomes unstable and develops the beads-on-string structure (Bhat *et al.* [5]) where droplets of fluid are held together by thin filaments of fluid in which the polymers are highly extended, before ultimately undergoing breakup. In regime 3, an extremely long ligament is generated that is still attached to the nozzle when the main drop is 1 mm away. The polymers in the ligament are close to their finite extension limit, indicating that extensional viscosity dominates the fluid

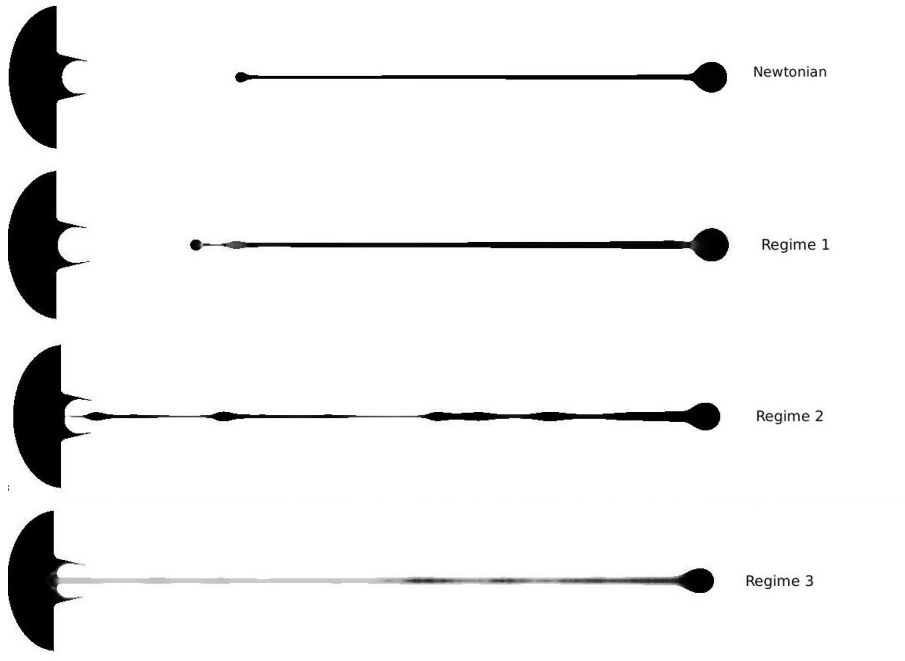


Fig. 10. Newtonian simulation with fluid viscosity 0.02 Pa.s. Simulations of polystyrene in DEP jetted from a Xaar print head; regime 1 (3% $M_w = 50$ kDa), regime 2 (0.095% $M_w = 200$ kDa) and regime 3 (0.003% $M_w = 2000$ kDa) shown when the main drop is 1 mm from the nozzle exit.

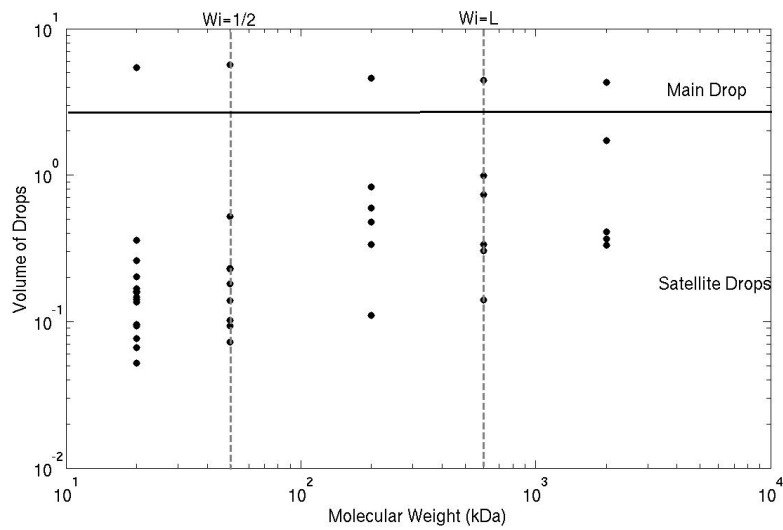


Fig. 11. Volume distribution of drops produced in simulations of jetting polystyrene in DEP through a Xaar print head for molecular weights spanning the three jetting regimes.

behaviour in this regime causing the fluid to act like a suspension of rigid rods. The high extensional viscosity limits the capillary instability.

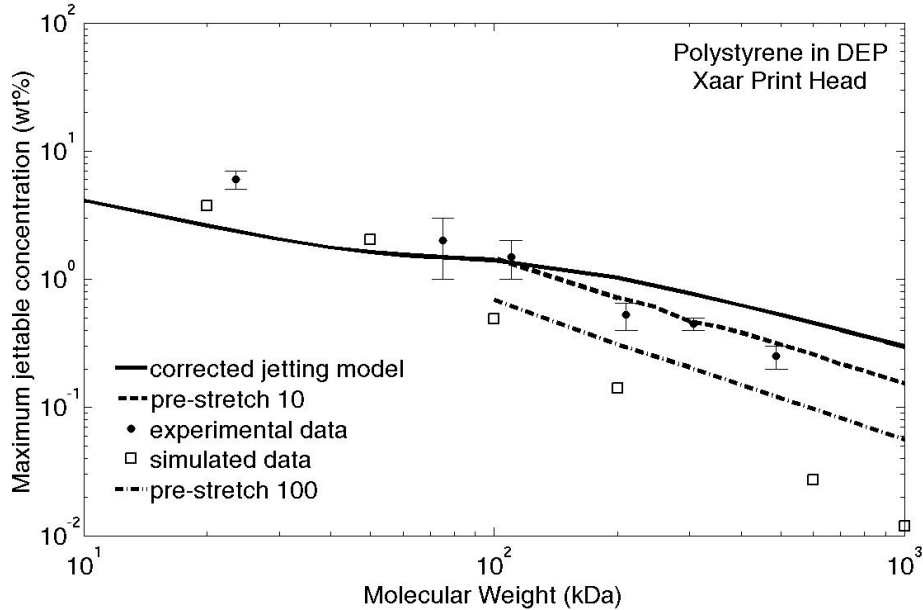


Fig. 12. Maximum jettable concentration (wt%) of polystyrene in DEP from a Xaar print head predicted by the corrected jetting model (line), the corrected jetting model modified pre-stretch factor 10 (dash line) and factor 100 (dot-dash line) simulations (square) and experimental data (circles).

The satellite drop volume distribution for a range of molecular weights spanning each of the jetting regimes is shown in Figure 11. At this Ohnesorge number, the low molecular weight solution breaks up into numerous, small satellite droplets, whereas, at high molecular weights fewer but larger satellite drops are generated. For example, Figure 11 shows that the number of satellite drops is reduced from 16 relatively small drops in jetting regime 1 (with nearly half having volume < 0.1) to 4 larger drops in jetting regime 3.

Figure 12 shows the maximum jettable concentration (wt%) predicted by the axisymmetric simulations compared to the corrected jetting model results. Again, we see that the jetting model overestimates the jettable concentration predicted by the simulations, as well as the experimental data. As discussed earlier, one cause may be due to the pre-stretching of the polymer molecules in the print head prior to exiting the nozzle.

4.3 Calculating Pre-stretch from Axisymmetric Simulations

We define the average initial value of A_{zz} for a cross-section radius a to be

$$\widehat{A_{zz}^0} = \frac{2}{a^2} \int_0^a r A_{zz}^0 dr, \quad (17)$$

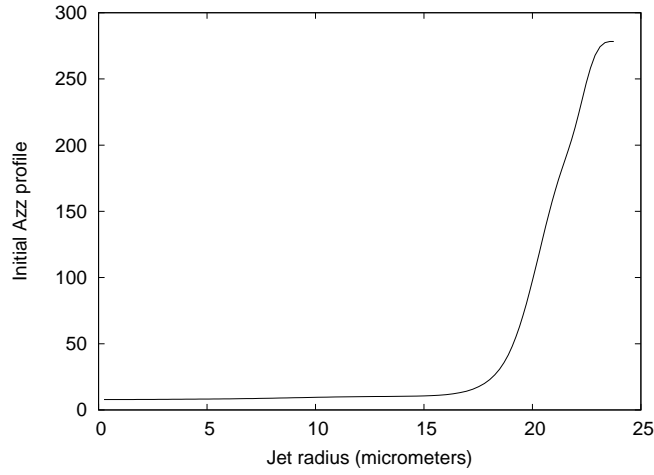


Fig. 13. Simulation of initial A_{zz}^0 profile across the nozzle exit generated by jetting a polymer of molecular weight $M_w = 2000$ kDa through a Xaar nozzle $D = 50 \mu\text{m}$ at initial speed $U_0 = 12$ m/s.

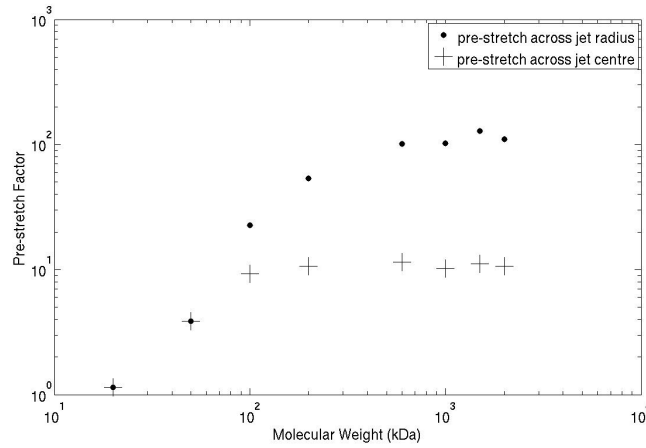


Fig. 14. Pre-stretch factor from simulations of jetting polystyrene in DEP through a Xaar print head calculated by equation (17) across the entire jet radius (dot) and across the jet centre (plus).

where A_{zz}^0 is the value of A_{zz} at the positions along the nozzle exit. This pre-stretch factor is calculated from our simulations for a range of molecular weights spanning each jetting regime.

The A_{zz}^0 profile is not uniform across the jet radius, but is shown in Figure 13 to increase steeply in a thin boundary layer close to the outer edge of the jet. Figure 14 demonstrates that there is a large difference in the pre-stretch

factor calculated for the entire jet radius compared to that calculated for a central section of the jet that excludes the high stress boundary. Stretching in this central section of the jet is attributed to the contraction flow into the nozzle, whereas the high stress region at the outer edge of the jet is due to the stretching of the free surface. In both cases the pre-stretch factor increases with molecular weight indicating that polymers are indeed stretched out to some degree inside the print head. As molecular weight increases, the degree to which the polymers can uncoil via the pre-stretch mechanism is limited. For example, the pre-stretch factor calculated across the centre of the jet reaches a maximum value of ~ 10 as molecular weight increases, due to the limited strain available through the contraction. Including the high stress boundary, the pre-stretch factor reaches a maximum value of ~ 100 .

The presence of a high stress boundary layer has been observed in simulations of a filament stretching device (Bhat *et al.* [6] and Yao & McKinley [38]), in which a polymeric liquid filament is extended between two end plates. An area of concentrated stress develops in a thin layer near to the fluid-air interface at the mid-point of the filament and remains even when a homogeneous extensional strain is reached. This is due to the viscoelastic memory of the fluid to its deformation history.

Excluding the high stress boundary by choosing the initial condition $A_{zz}^0 = 10$ gives a quantitative agreement between the corrected jetting model results and the experimental data, as seen by the dashed line in Figure 12. However, we also observe that the axisymmetric simulations underestimate the jettable concentration. This discrepancy is probably the result of differences in the print head geometry between the axisymmetric simulations and the actual highly non-axisymmetric print head. However, a second possible explanation is that the polymers are being fractured due to the high stresses.

5 Polymer Scission during Jetting

5.1 Fracturing Polymer Molecules

Evidence of polymer scission occurring in inkjet printing was recently reported by A-Alamry *et al.* [1] in jetting experiments, in which approximately monodisperse polystyrene solutions were jetted through two different print heads. They examined the molecular weight distributions of polymer before and after jetting. In the faster Dimatix print head, they found a change in the molecular weight distribution corresponding to an increase in the fraction of polymers of half the mean molecular weight, but the distribution remained unchanged when using the Microfab printer, which is much slower and has a wider nozzle

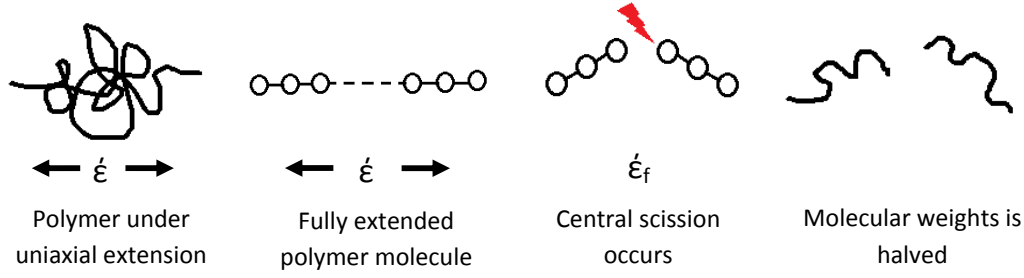


Fig. 15. Central scission of a fully extended polymer molecule when the strain rate $\dot{\epsilon}$ of the flow exceeds the fracture strain rate $\dot{\epsilon}_f$ given by equation (18).

diameter. Full details of the two print heads are given later.

Halving of the molecular weight distribution indicates that the polymer is broken into two equally sized chains during the jetting process. This mechanism is known as central scission. Although there may be some circumstances where reducing the molecular weight during printing may be advantageous, flow-induced degradation is a serious problem in jetting applications involving functional organic materials, where damage to the molecular structure will prevent the molecules from functioning correctly.

Odell & Keller [30] showed that flow induced central scission of high molecular weight polymers can occur in the high-strain extensional flow produced by an opposed jet. A polymer molecule will fracture if the tension force at the centre of a fully extended polymer molecule exceeds the carbon-carbon bond force. For polystyrene in ATP this gives a critical fracture strain rate [30] of

$$\dot{\epsilon}_f = \frac{7.24 \times 10^{17}}{M_w^2} \text{ s}^{-1}, \quad (18)$$

for molecular weight measured in Daltons (Da). This is a decreasing function of molecular weight indicating that higher molecular weight polymers are easier to fracture. For a molecule to undergo central scission, the polymer must be both fully extended (i.e. in jetting regime 3) and the the strain rate of the flow must overcome this fracture condition (18).

In order to investigate whether the conditions for central scission exist within inkjet printing, we consider the strain rate of the flow at two locations; in the ligament when the polymers become fully extended and at the nozzle exit. These strain rates are illustrated in Figure 16. The critical strain rate at which the polymers are at full extension in the ligament is defined to be

$$\dot{\epsilon}_{crit} = \frac{U_{crit}}{Z_{crit}} \text{ s}^{-1}, \quad (19)$$

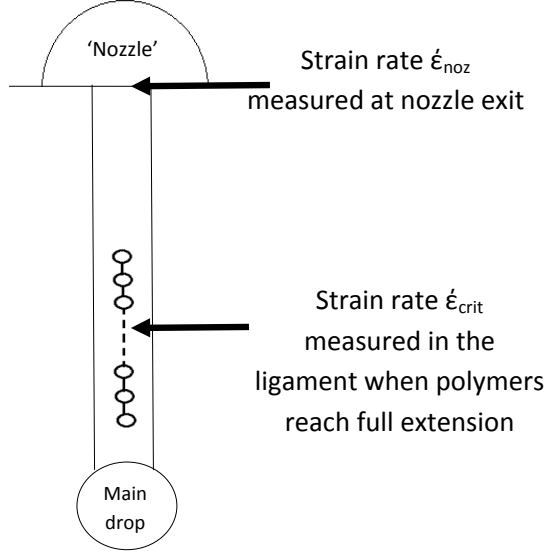


Fig. 16. Critical strain rate $\dot{\epsilon}_{crit}$ given by equation (19) compared to the strain rate measured at the nozzle $\dot{\epsilon}_{noz}$ given by equation (20) in the jetting model.

where critical values are defined at maximum axial stress. The strain rate at the nozzle exit is defined as

$$\dot{\epsilon}_{noz} = 8 \frac{U_0}{D} \text{ s}^{-1}, \quad (20)$$

on the assumption of fully developed Poiseuille flow in the nozzle.

5.2 Polystyrene/ATP Solution jetted using the Dimatix Print head

A-Alamry *et al.* [1] examined the changes to the molecular weight distribution of polystyrene dissolved in ATP for two different print systems. First the solution is jetted at $U_f = 10$ m/s from a $23 \mu\text{m}$ diameter nozzle using a Dimatix DMP-2800 10Pl print head. We assume that the ratio between the final print speed and the speed at which the ink exits the nozzle is 3. Thus, the speed used in the jetting model is $U_0 = 30$ m/s. The jetting conditions and fluid parameters are listed in Table 5. A-Alamry *et al.* find that central scission occurs for the molecular weight range $290 < M_w < 770$ kDa under these conditions.

Figure 17 shows the evolution of the axial configuration component A_{zz} compared to the finite extensibility limit L^2 as ligament length increases for a

Solvent	ATP	Nozzle	Dimatix
solvent viscosity, μ_s	0.0017Pa.s	nozzle diameter, D	23 μm
solvent quality, ν	0.59	initial speed, U_0	30 m/s
fluid density, ρ	1028 kg/m ³	print speed, U_f	10 m/s

Table 5

Fluid parameters and jetting conditions for polystyrene in ATP jetted from a Dimatix DMP-2800 10pl print head.

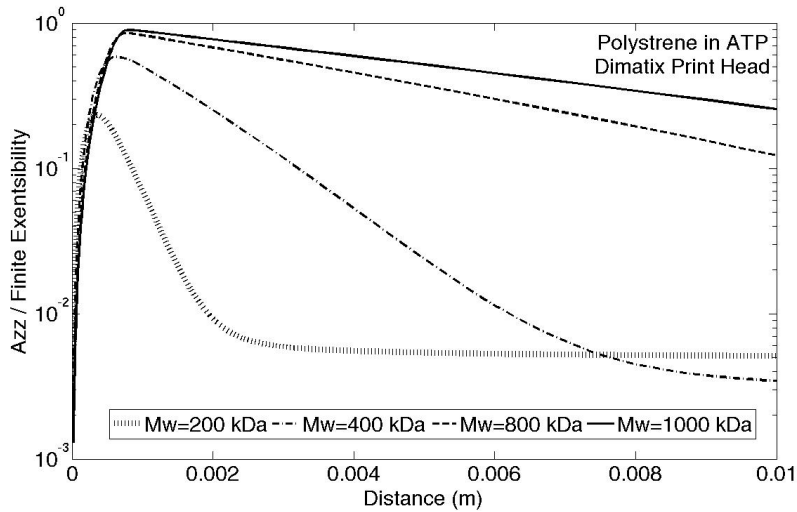


Fig. 17. A_{zz}/L^2 profiles for molecular weight range $M_w = 200 - 1000$ kDa for polystyrene in ATP jetted from a Dimatix print head.

number of molecular weights. The change in behaviour from the viscoelastic regime to the fully extended regime, in which the non-linear spring dominates, is evident as molecular weight is increased. In particular, for $M_w = 1000$ kDa, $A_{zz} \sim L^2$ indicating that the polymer has reached full extension. For a sufficient strain rate, the tension force may exceed the strength of the chain bond leading to fracture of the polymer backbone. The jetting model can be used to determine whether the strain rate is large enough for this degradation to occur.

We calculate that the transition from regime 2 to regime 3 occurs at $M_w = 256$ kDa and is plotted in Figure 18. There exists a range of molecular weights, within jetting regime 3, where polymers will become fully extended under these jetting conditions. However, the strain rate at full extension given by equation (19) is not large enough to fracture the polymer molecules, as shown in Figure 18. Hence, we can conclude that the extensional flow in the ligament

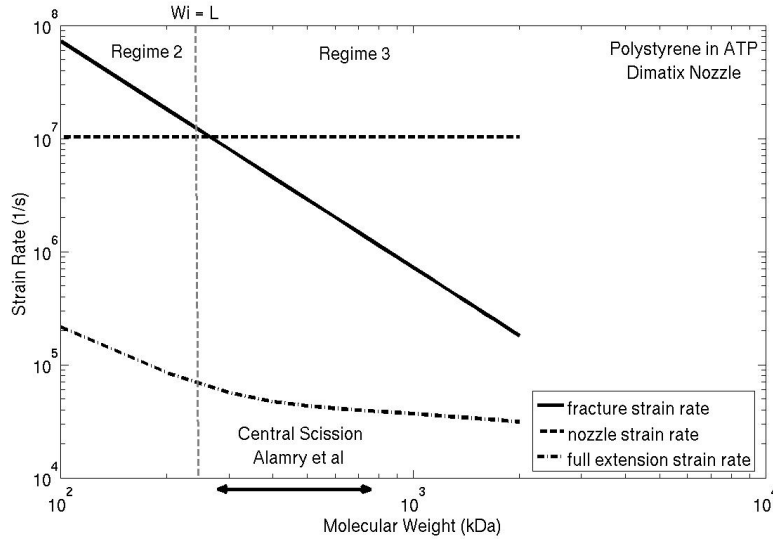


Fig. 18. Fracture strain rate (18) (solid), nozzle strain rate (20) (dashed) and critical strain rate (19) (dash-dot) for the Dimatix nozzle with the transition from regime 2 to 3 (dashed). The arrow indicates the range of M_w for which central scission is reported [1].

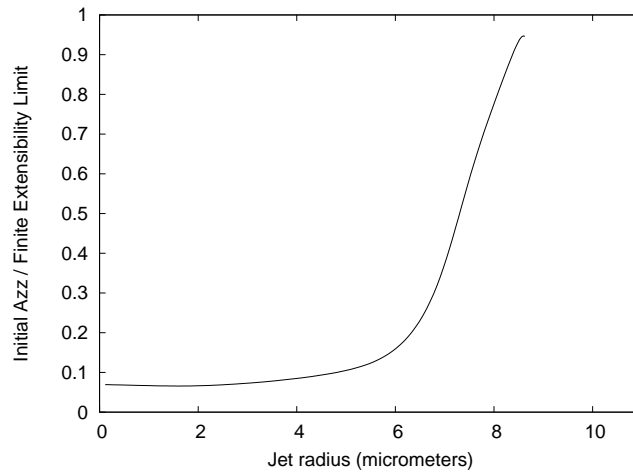


Fig. 19. Simulation of A_{zz}^0/L^2 across the nozzle exit generated by jetting a polymer of molecular weight $M_w = 500$ kDa through a Dimatix nozzle $D = 23 \mu\text{m}$ at reduced speed $U_0 = 10\text{m/s}$.

of the DoD jet is not strong enough to cause central scission.

On the other hand Figure 18 also suggests that the nozzle strain rate given by equation (20) is sufficient to exceed the fracture condition. Thus, polymers will undergo central scission at the nozzle exit, provided that the molecules have

become fully extended within the nozzle. Our axisymmetric simulations in section 4 have demonstrated that significant stretching occurs within a print head with a sudden contraction. Figure 19 demonstrates the high stress boundary layer near to the free surface. Furthermore, the initial axial configuration A_{zz}^0 is near to the upper limit L^2 in this region, suggesting that the polymers are near to their finite extension limit as the fluid exits the nozzle.

Modelling suggests that under the conditions present in the Dimatix print head used in the experiments of A-Alamry *et al.* [1], a proportion of the molecules will become both fully extended and subjected to a sufficient strain rate at the nozzle exit such that central scission can occur. Hence, we can conclude that the mechanism responsible for central scission under DoD jetting conditions is likely to be the high strain rate at the nozzle exit rather than the extensional flow in the jet. A-Alamry *et al.* observe central scission occurs in the molecular weight range $290 < M_w < 770$ kDa. The lower boundary coincides with the transition to regime 3, as well as the nozzle strain rate overcoming the fracture condition. The upper boundary is possibly due to these very large molecules being unable to their uncoil to full extension within the nozzle.

5.3 Polystyrene/ATP Solution jetted using the Microfab Print head

A-Alamry *et al.* [1] also studied jetting at $U_f = 5$ m/s through a $50 \mu\text{m}$ diameter nozzle using a Microfab micropipette system. Recall that the micropipette nozzle is smooth and tapered compared to the sudden contraction of the Dimatix nozzle and so are unlikely to cause pre-stretch in the nozzle. In contrast to the Dimatix print head, A-Alamry *et al.* do not observe central scission with this system.

Solvent	ATP	Nozzle	Microfab
solvent viscosity, μ_s	0.0017Pa.s	nozzle diameter, D	$50 \mu\text{m}$
solvent quality, ν	0.59	initial speed, U_0	15 m/s
fluid density, ρ	1028 kg/m ³	print speed, U_f	5 m/s

Table 6

Fluid parameters and jetting conditions for polystyrene in ATP jetted from a Microfab micropipette system.

In Figure 20, we show that the strain rate at the nozzle exit and the strain rate at full extension, on the assumption that the fluid velocity at the exit is 3 times the final velocity i.e. $U_0 = 15$ m/s. Details of the jetting conditions and fluid parameters are given in Table 6.

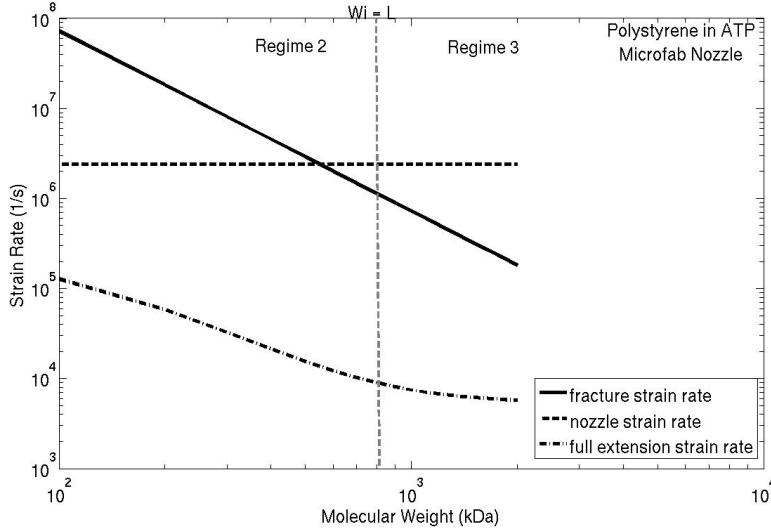


Fig. 20. Fracture strain rate (18) (solid), nozzle strain rate (20) (dashed) and critical strain rate (19) (dash-dot) the Microfab nozzle with the transition from regime 2 to 3 (dashed).

Again we see that the strain rate in the ligament is too small to cause fracture. On the other hand, although the strain rate at the nozzle is lower than the Dimatix system, it is still sufficient to induce central scission for molecular weights $M_w > 500$ kDa. However, unlike the Dimatix head, the Microfab print head does not have a sudden contraction and therefore it is unlikely that the polymers will become fully extended in the nozzle. A-Alamry *et al.* do not observe central scission in this case.

6 Conclusions

In this paper we have tested the predictions of the simple model of jetting given by Hoath *et al.* against both experimental observations and full numerical simulations. For a low viscosity solvent (ATP), where the molecular weight corresponding to a relaxation rate equal to the initial strain rate is large, we are able to identify all three of the asymptotic regimes identified by Hoath *et al.*. Furthermore, the predictions of the model agree quantitatively with the experiments of de Gans *et al.* [18] using a micropipette system. However, for the higher viscosity DEP system jetted through an industrial print head, we don't observe the middle scaling regime and there is a significant discrepancy from the experimental results.

We have identified three factors that contribute to these discrepancies. First, for the DEP system of Hoath *et al.* [24], where jetting of low molecular weight

polymers is possible at concentrations above ϕ^* , the Zimm model underestimates the relaxation time and therefore both polymer contribution viscosity and the Weissenberg number. Second, the abrupt contraction of the industrial print head compared to the gently tapering micropipette nozzle produces a significant pre-stretch of the polymers that is not accounted for in the model. When these effects are included, the model produces predictions similar to the full numerical simulations and the experimental data. Finally, there is possibility, already identified by A-Alamry *et al.* [1], that polymers are degraded due to flow-induced scission. Our modelling suggests that this does not occur as a result of the extensional flow in the ligament, but rather as a consequence of the high strains and strain rates in the nozzle and so could be avoided by changing the nozzle geometry.

Acknowledgments

This work was supported by the UK Engineering and Physical Sciences Research (EPSRC) through grant number EP/H018913/1 Innovation in Industrial Ink-jet Technology. We would like to thank Dr Stephen Hoath from the University of Cambridge for helpful discussions.

References

- [1] A-Alamry K., Nixon K., Hindely R., Odell J.A. and Yeates S.G., “Flow-Induced Polymer Degradation During Ink-Jet Printing” *Macromol. Rapid Commun.* 32 (2011) 316–320
- [2] Ambravaneswaran B., Wilkes E.D. and Basaran O.A., “Drop formation from a capillary tube: Comparison of one-dimensional and two-dimensional analyses and occurrence of satellite drops” *Phys. Fluids* 14 (2002) 2606–2621
- [3] Basaran O.A., Haijing G. and Bhat P.P, “Nonstandard Inkjets” *Annu. Rev. Fluid Mech.* 45 (2013) 85–113
- [4] Bazilevskii A.D., Meyer J.D. and Rohzkov A.N., “Dynamics and breakup of pulse microjets of polymeric liquids” *Fluid Dyn.* 29 (2005) 381–432
- [5] Bhat P.P, Appathurai S., Harris M.T., Pasquali M., McKinley G.H. and Basaran O.A., “Formation of beads-on-a-string structures during breakup of viscoelastic filaments” *Nature Phys.* 6 (2010) 625–631
- [6] Bhat P.P., Basaran O.A. and Pasquali M., “Dynamics of viscoelastic liquid filaments: Low capillary number flows” *J. Non-Newt. Fluid Mech.* 150 (2008) 211–225

- [7] Castrejón-Pita J.B., Morrison N.F., Harlen O.G., Martin G.D. and Hutchings I.M., “Experiments and Lagrangian simulations on the formation of droplets in drop-on-demand mode” *Phys. Rev. E* 83 (2011) 036306
- [8] Chen A.U. and Basaran O.A., “A new method for significantly reducing drop radius without reducing nozzle radius in drop-on-demand drop production” *Phys Fluids* 14 (2002) 1–4
- [9] Chilcott M.D., Rallison J.M., “Creeping Flow of Dilute Polymer Solutions Past Cylinders and Spheres” *J. Non-Newt. Fluid Mech.* 29 (1988) 381-432
- [10] Clanet C. and Lasheras J.C., “Transition from dripping to jetting” *J. Fluid Mech.* 383 (1999) 307–326
- [11] Clasen C., Plog J.P., Kulicke W.M., Owens M., Macosko C., Scriven L.E., Verani M. and McKinley G.H., “How dilute are dilute solutions in extensional flows?” *J. Rheol.* 50 (2006) 849–881
- [12] Clasen C., Bico J., Entov V. and McKinley G.H., “‘Gobbling drops’: the jetting/dripping transition in flows of polymer solutions” *J. Fluid Mech.* 636 (2009) 5–40
- [13] Derby B., “Inkjet Printing of Functional and Structural Materials: Fluid Property Requirements, Feature Stability and Resolution” *Annu. Rev. Mater. Res.* (2010) 395–414
- [14] Dong H., Carr W.W. and Morris J.F. “An experimental study of drop-on-demand drop formation” *Phys. Fluids* 18 (2006) 072102
- [15] Eggers J. and Dupont T.F. “Drop formation in a one-dimensional approximation of the Navier-Stokes equation” *J. Fluid Mech.* 262 (1994) 205–221
- [16] Eggers J. and Villermaux E., “Physics of liquid jets” *Rep. Prog. Phys.* 71 (2008) 036601
- [17] Feng J.Q. “A general fluid dynamics analysis of drop ejection in drop-on-demand ink jet devices” *J. Imaging Sci. tech.* 46 (2002) 398–408
- [18] de Gans B.J., Kazancioglu E., Meyer W. and Schubert U.S., “Inkjet printing polymers and polymer libraries using micropipettes” *Macromol. Rapid Commun.* 25 (2004) 292–296
- [19] de Gans B.J., Duineveld P.C. and Schubert U.S., “Inkjet Printing of Polymers: State of the Art and Future Developments” *Adv. Matter* 16 (2004) 203–213
- [20] de Gans B.J., Xue L., Agarwal U.S. and Schubert U.S., “Inkjet Printing of Linear and Star Polymers” *Macromol. Rapid Commun.* 26 (2005) 310–314
- [21] Harlen O.G., Rallsion J.M. and Szabo P., “A split Lagrangian-Eulerian method for simulationg transient viscoelastic flows” *J. Non-Newt. Fluid Mech.* 60 (1995) 81–104

- [22] Hoath S.D., Martin G.D., Castrejon-Pita J.R. and Hutchings I.M., “Satellite formation in drop-on-demand printing of polymer solutions” *Society for Imaging Science and Technology* 23 (2007) 331-335
- [23] Hoath S.D., Hsiao W., Jung S., Martin G.D. and Hutchings I.M., “Dependence of Drop Speed on Nozzle Diameter, Viscosity and Drive Amplitude in Drop-on-Demand Inkjet Printing” *Proc. NIP27* (2011) 62–65
- [24] Hoath S.D., Harlen O.G. and Hutchings I.M., “Jetting behaviour of polymer solutions in drop-on-demand inkjet printing” *J. Rheology* 56 (2012) 1109
- [25] Hutchings I.M. and Martin G.D., “Inkjet Technology For Digital Fabrication” A John Wiley & Sons Ltd. Chichester (2013)
- [26] Martin G.D., Hoath S.D. and Hutchings I.M., “Inkjet printing - the physics of manipulating liquid jets and drops” *J. Phys. Conf. Ser.* 105 (2008) 012001
- [27] McKinley G.R. and Renardy M., “Wolfgang von Ohnesorge” *Phys. Fluids* 23 (2011) 127101
- [28] Morrison N.F. and Harlen O.G., “Viscoelasticity in inkjet printing” *Rheol. Acta* 49 (2010) 619–632
- [29] Muller A.J., Odell J.A. and Keller A., “Polymer degradation in extensional flow” *Polym. Commun.* 30 (1989) 298-301
- [30] Odell J.A. and Keller A., “Flow-Induced Chain Fracture of Isolated Linear Macromolecules in Solution” *J. Polym. Sci. Part B: Poly. Phys.* 24 (1986) 1889–1916
- [31] Shore H.J. and Harrison G.M., “The effect of added polymer on the formation of drops ejected from a nozzle” *Phys. Fluids* 17 (2005) 033104
- [32] Szabo P., McKinley G.H. and Clasen C., “Constant force extensional rheometry of polymer solutions” *J. Non-Newt. Fluid Mech.* 169 (2012) 26–41
- [33] Vadillo D.C., Matthues W. and Clasen C. “Microsecond relaxation processes in shear and extensional flows of weakly elastic polymer solutions” *Rheol. Acta.* 51 (2012) 755–769
- [34] Westborg H. and Hassager O., “Creeping motion of long bubbles and drops in capillary tubes” *J. Colloidal and Interface Science* 133 (1989) 135–147
- [35] Wilkes E.D., Phillips S. D. and Basaran O.A. “Computational and experimental analysis of dynamics of drop formation” *Phys. Fluids* 11 (1999) 3577–3598
- [36] Xu D., Sanchez-Romaguera V., Barbosa S., Travis W., de Wit J., Swan P. and Yeates S.G. “Ink-jet printing of polymer solutions and the role of chain entanglement” *J. Mater. Chem.* 17 (2007) 4902–4907
- [37] Xu Q. and Basaran O.A. “Computational analysis of drop-on-demand drop formation” *Phys. Fluids* 19 (2007) 102111

- [38] Yao M. and McKinley G.H., “Numerical simulation of extensional deformations of viscoelastic liquid bridges in filament stretching devices” *J. Non-Newt. Fluid Mech.* 74 (1998) 47–88